Geophys. J. Int. (2004) **156,** 467–482 doi: 10.1111/j.1365-246X.2004.02178.x

Near-field influence on shear wave splitting and traveltime sensitivity kernels

Noémie Favier, Sébastian Chevrot and Dimitri Komatitsch

Laboratoire de Dynamique Terrestre et Planétaire, UMR 5562*, Observatoire Midi-Pyrénées,* 14, *av. Edouard Belin,* 31400 *Toulouse, France.*
E-mail: favier@pontos.cst.cnes.fr

Accepted 2003 October 20. Received 2003 September 15; in original form 2003 May 15

SUMMARY

In the last few years, Fréchet (or sensitivity) kernels for seismic traveltimes have become important tools for mantle tomography. Sensitivity kernels for splitting intensity have been introduced recently for a better interpretation of shear wave splitting measurements. All ray-based sensitivity kernels studies relied so far on a far-field approximation of the Green's tensor. Under this approximation, the sensitivity kernels for splitting intensity do not accurately describe shear wave splitting at shallow depth. Here, we investigate the influence of near-field terms of the Green's tensor on the sensitivity kernels for both splitting intensity and traveltimes. Using the Born approximation, we derive analytical expressions for the complete sensitivity kernels. In contrast to the kernels obtained from the far-field Green's tensor, the sensitivity kernels based upon the complete Green's tensor are no longer zero on the ray path and show a complicated structure near the receiver. The results show that the near-field terms are needed to get accurate kernels at shallow depth. Using the complete Green's tensor, we define the normalized depth interval where near-field terms are important.

Key words: anisotropy, near-field, sensitivity kernels, shear wave splitting, traveltimes.

1 INTRODUCTION

Most tomographic studies of seismic traveltimes are based on classical ray theory. Under this approximation, the arrival time of a seismic body wave depends only on the wave speed along the geometric ray path between the source and the receiver. Ray theory is strictly valid only at infinite frequency. As a consequence of their finite frequency bandwidth, seismic waves are sensitive to broad structures in the vicinity of the ray path. Recently, seismologists have begun to investigate 3-D propagation of seismic waves to better understand how waves sample the medium in which they propagate. Following this approach, Marquering *et al.* (1998), Marquering *et al.* (1999), Zhao & Jordan (1998), Zhao *et al.* (2000), Dahlen *et al.* (2000) and Hung *et al.* (2000) determined 3-D sensitivity kernels for both travel times and waveforms. They came to the important and counter-intuitive conclusion that delay time is not sensitive to the structure along the ray path and that waves have significant sensitivity outside the source-receiver plane. Recently, Favier & Chevrot (2003) derived the analytical expression of sensitivity kernels for shear wave splitting in transverse isotropic media under the Born approximation. They described shear wave splitting based on a new seismic observable called 'splitting intensity' (Chevrot 2000). Splitting intensity depends on the angle between the polarization of the incoming wave and the fast-axis direction, and is directly proportional to the differential traveltime between the two quasi-shear waves. Sensitivity for splitting intensity is zero along the ray path, like the sensitivity for traveltime.

To our knowledge, all previous ray-based calculations of sensitivity kernels have relied on a far-field approximation, assuming that seismic scattering occurs at distances from the source and from the station that are much larger than the wavelength. Favier & Chevrot (2003) noticed that under this approximation, the sensitivity kernels do not accurately describe shear wave splitting at shallow depths. In the present article, we use the complete Green's tensor to derive the full sensitivity kernels for splitting intensity and traveltimes. These kernels differ from the kernels calculated from the far-field contribution alone. Next, we consider a vertically propagating plane wave in a transversely isotropic medium to compute the sensitivity kernels for splitting intensity, and in an isotropic medium to compute the sensitivity kernels for delay times. Then, we determine the depth averaged sensitivity kernels. Finally, we use the spectral-element method to generate synthetic seismograms to validate our results.

2 SENSITIVITY KERNELS DERIVATION

2.1 General expressions of Fréchet kernels

By definition, Fréchet kernels provide a linear relation between perturbations of the medium and some seismic observable. In this article, we focus on two seismic observables: traveltime and splitting intensity.

2.1.1 Traveltimes

The delay time Fréchet kernel or Fréchet derivative is the linear operator that associates the first-order traveltime anomaly δT to an arbitrary perturbation $\delta p(\mathbf{r})$ (Tarantola 1987). Let $K_p(\mathbf{r}_0; \mathbf{r})$ be the Fréchet kernel at $\mathbf{r}$ for a receiver at $\mathbf{r}_0$ for the parameter p. Then we have:

$$\delta T(\mathbf{r}_0) = \int_V K_p(\mathbf{r}_0; \mathbf{r}) \delta p(\mathbf{r}) d^3\mathbf{r}. \tag{1}$$

The integral is over the entire volume of the Earth. At the receiver, the delay time is defined by the scalar product of the time derivative of the initial wavefield $\dot{u}_0(t)$ and the perturbed wavefield $\delta u(t)$, which gives (Dahlen *et al.* 2000; Zhao *et al.* 2000):

$$\delta T = \frac{\int_{-\infty}^{+\infty} \dot{u}_0(t) \delta u(t)\, dt}{\int_{-\infty}^{+\infty} \ddot{u}_0(t) u_0(t)\, dt}. \tag{2}$$

Let us note that a negative delay time anomaly δT corresponds to an advance in the arrival of the perturbed wave with respect to the incident wave, whereas a positive delay time corresponds to a delay.

2.1.2 Splitting intensity

As a shear wave propagates in an anisotropic medium, it splits into two orthogonally polarized quasi-shear waves that propagate at different phase velocities. In the simple case of a symmetry-axis lying in the horizontal plane, Favier & Chevrot (2003) showed that splitting intensity measured at the surface depends linearly on the model parameters γ_c and γ_s derived from the anisotropic parameter $\gamma = (\delta c_{1212} - \delta c_{2323})/2c_{2323}$ (Mensch & Rasolofosaon 1997) so that $\gamma_c = \gamma \cos 2\phi_0$ and $\gamma_s = \gamma \sin 2\phi_0$ with ϕ_0 the direction of the fast-axis. The Fréchet kernels for splitting intensity provide linear integral relationships between splitting intensity S and variations of the parameters γ_c and γ_s:

$$S(\mathbf{r}_0) = \int_V K_{\gamma_c}(\mathbf{r}_0; \mathbf{r}) \gamma_c(\mathbf{r})\, d^3\mathbf{r} + \int_V K_{\gamma_s}(\mathbf{r}_0; \mathbf{r}) \gamma_s(\mathbf{r})\, d^3\mathbf{r}, \tag{3}$$

where $K_{\gamma_c}(\mathbf{r}_0; \mathbf{r})$ and $K_{\gamma_s}(\mathbf{r}_0; \mathbf{r})$ are the Fréchet kernels at $\mathbf{r}$ for a receiver at $\mathbf{r}_0$. Chevrot (2000) defined splitting intensity as the scalar product of the transverse component $\delta u^T(t)$ (produced by the anisotropic part of the stiffness tensor) and the time derivative of the radial component $\dot{u}_0^R(t)$:

$$S = -2 \frac{\int_{-\infty}^{+\infty} \dot{u}_0^R(t) \delta u^T(t)\, dt}{\int_{-\infty}^{+\infty} |\dot{u}_0^R(t)|^2\, dt}. \tag{4}$$

Splitting intensity is proportional to the amplitude of the transverse component, and both quantities depend on the time delay accumulated between the fast and slow quasi-shear waves. Expressions (2) and (4) are similar. The main difference is that the displacement field perturbation in (2) has the same polarization as $\mathbf{u^R}$, whereas it is polarized orthogonally to $\mathbf{u^R}$ in (4). Using the Born approximation, we derive the perturbed displacement field in both cases.

2.2 Born approximation

Let us consider a reference isotropic medium. We can write the total wavefield as the sum of the wavefield in the reference isotropic medium and a perturbation resulting from scattering of the reference wavefield by the elastic (isotropic or anisotropic) heterogeneities in the medium. Using the Born approximation, the perturbed field recorded by the receiver at $\mathbf{r}_0$ is a function of the elastic perturbation at each point $\mathbf{r}$ and is given by the secondary point source terms δf_j (Favier & Chevrot 2003):

$$\delta f_j = \frac{\partial}{\partial x_i} \left(\delta c_{ijkl} \frac{\partial u_k}{\partial x_l} \right). \tag{5}$$

This source term describes the scattering of the reference wavefield by a perturbation of the stiffness tensor at a given point $\mathbf{r}$ of the medium. Using the Green's tensor representation, we write the perturbed field:

$$\delta u_n(\mathbf{r}_0, t) = -\int_V \frac{\partial G_{np}}{\partial x_q}(\mathbf{r}_0, t; \mathbf{r}) * \left[\delta c_{pqij} \frac{\partial u_i(\mathbf{r}, t)}{\partial x_j} \right] d^3\mathbf{r}, \tag{6}$$

where * denotes convolution. Using eqs (2) and (4) and the perturbations δu_n given by (6), one can compute the sensitivity kernels.

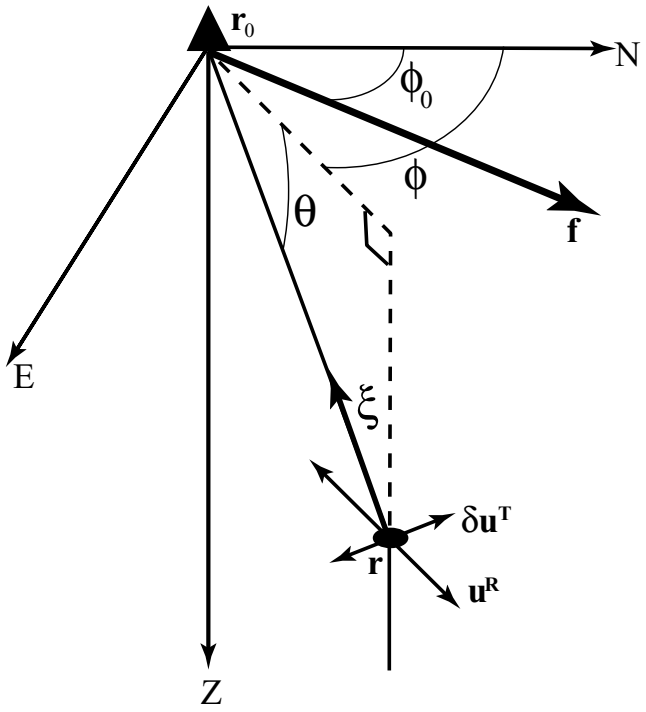

Figure 1. Notations used to describe seismic scattering. The symmetry-axis is represented by axis **f**. The scattering point is located at **r**. The unit vector $\boldsymbol{\zeta}$, travelling from the scattering point at **r** to the receiver at $\mathbf{r}_0$, has an azimuth ϕ and an elevation from the horizontal plane θ. The vector $\mathbf{u^R}$ is the initial polarization of the incident wave and $\boldsymbol{\delta u^T}$ is the scattered transverse component orthogonal to $\mathbf{u^R}$.

2.3 The full Green's tensor

The Green's tensor is the solution of the equation:

$$\rho \frac{\partial^2}{\partial t^2} G_{\text{in}} = \delta_{\text{in}} \delta(\mathbf{r}) \delta(t) + \frac{\partial}{\partial x_j} \left(c_{ijkl} \frac{\partial}{\partial x_l} G_{kn} \right). \tag{7}$$

In a reference unbounded homogeneous isotropic medium, eq. (6) can be developed as (Aki & Richards 1980 eq. 4.29):

$$\begin{aligned}
\delta u_n(\mathbf{r}_0, t; \mathbf{r}) = & \frac{15\zeta_n\zeta_p\zeta_q - 3\zeta_n\delta_{pq} - 3\zeta_p\delta_{nq} - 3\zeta_q\delta_{np}}{4\pi\rho} \frac{1}{r^4} \int_{r/\alpha}^{r/\beta} \tau M_{pq}(\mathbf{r}, t-\tau)\, d\tau \\
& - \frac{6\zeta_n\zeta_p\zeta_q - \zeta_n\delta_{pq} - \zeta_p\delta_{nq} - 2\zeta_q\delta_{np}}{4\pi\rho\beta^2} \frac{1}{r^2} M_{pq}(\mathbf{r}, t - r/\beta) \\
& + \frac{6\zeta_n\zeta_p\zeta_q - \zeta_n\delta_{pq} - \zeta_p\delta_{nq} - \zeta_q\delta_{np}}{4\pi\rho\alpha^2} \frac{1}{r^2} M_{pq}(\mathbf{r}, t - r/\alpha) \\
& + \frac{\zeta_p\zeta_q\zeta_n}{4\pi\rho\alpha^3} \frac{1}{r} \dot{M}_{pq}(\mathbf{r}, t - r/\alpha) \\
& - \frac{\zeta_n\zeta_p - \delta_{np}}{4\pi\rho\beta^3} \zeta_q \frac{1}{r} \dot{M}_{pq}(\mathbf{r}, t - r/\beta),
\end{aligned} \tag{8}$$

where $M_{pq}(\mathbf{r}, t) = \delta c_{pqij} \frac{\partial u_i(\mathbf{r},t)}{\partial x_j}$ is the seismic moment tensor induced by the secondary point source terms, $r = |\mathbf{r} - \mathbf{r}_0|$; $\boldsymbol{\zeta}$ the unit vector pointing from the scattering point **r** to the receiver $\mathbf{r}_0$ (see Fig. 1); and δ_{ij} the Kronecker's symbol. Terms α and β represent the P and S wave velocities in the isotropic reference medium, respectively.

The fourth and fifth terms on the right-hand side of (8) correspond to the far-field P and S waves, respectively. These contributions dominate the signal when the distance between the scattering point and the receiver is much larger than the wavelength. The second and third terms respectively describe the propagation of S and P waves in the middle-field (MF, $1/r^2$ decay). The first term represents the near-field contribution, which depends on both P and S waves. Because of the integral, this term can be split into two terms, one called the near-field term (NF, $1/r^3$ decay) and one called the local-field (LF, $1/r^4$ decay). Previous studies computed sensitivity kernels using the asymptotic form of the Green's tensor in the far-field approximation and considered the fourth and fifth terms only (Marquering *et al.* 1998, 1999; Dahlen *et al.* 2000; Favier & Chevrot 2003).

3 COMPLETE SENSITIVITY KERNELS

Using the full Green's tensor, we now derive complete sensitivity kernels for both splitting intensity and delay time in an unbounded homogeneous isotropic medium. We neglect the effects of the free surface and of multiple scattering. Section 5 shows that these effects are negligible compared to the influence of near-field and middle-field terms. The far-field term contribution to the sensitivity kernel for shear wave splitting is derived first. The other kernels can be obtained in similar ways.

3.1 Example: far-field term for shear wave splitting

Let us consider a plane *SKS* wave propagating vertically in a reference isotropic medium. Such a wave is radially polarized with a polarization direction corresponding to the backazimuth of the source ϕ_b. The displacement field at point $\mathbf{r}$ and at time t can be written in complex notation as:

$$\mathbf{u}^R(\mathbf{r},t) = \begin{pmatrix} \cos\phi_b \\ \sin\phi_b \\ 0 \end{pmatrix} u_0^R(\mathbf{r},t) = \begin{pmatrix} \cos\phi_b \\ \sin\phi_b \\ 0 \end{pmatrix} u_0 e^{i\omega(t+z/\beta)}$$

in the geographic coordinate system, with north and east axes in the horizontal plane and the Z-axis pointing down (see Fig. 1). The stiffness tensor for the reference medium is given by:

$$c_{ijkl} = \lambda\delta_{ij}\delta_{kl} + \mu(\delta_{ik}\delta_{jl} + \delta_{il}\delta_{jk}),$$

where P- and S-wave velocities are $\alpha = \sqrt{(\lambda+2\mu)/\rho}$ and $\beta = \sqrt{\mu/\rho}$ respectively. We consider transverse isotropic perturbations of the stiffness tensor given by:

$$\delta c_{2323} = \delta c_{1313} = -\delta c_{1212}.$$

The scattered wavefield produced by a transverse isotropic perturbation located at $\mathbf{r}$ and recorded at $\mathbf{r}_0$ is given by

$$\delta u_{n,S}^{FF}(\mathbf{r}_0,t;\mathbf{r}) = -\frac{\zeta_n\zeta_p - \delta_{np}}{4\pi\rho\beta^3}\zeta_q\frac{1}{r}\delta c_{pqij}\frac{\partial}{\partial t}\frac{\partial u_i(\mathbf{r},t-r/\beta)}{\partial x_j}.$$

The presence of transverse isotropic perturbations will result in energy on the transverse component. In the simple case where the symmetry-axis of the transverse isotropic medium lies in the horizontal plane, the scattered transverse component can be written as:

$$\delta u_S^{T,FF}(\mathbf{r}_0,t;\mathbf{r}) = \sin\phi_b\,\delta u_{1,S}^{FF}(\mathbf{r}_0,t;\mathbf{r}) - \cos\phi_b\,\delta u_{2,S}^{FF}(\mathbf{r}_0,t;\mathbf{r}) \tag{9}$$

$$= -\frac{\delta c_{2323}}{c_{2323}}F_S^{FF}(\theta,\phi,\phi_b,\phi_0)\frac{\omega^2}{4\pi\beta^2 r}u_0 e^{i\omega[t+(z-r)/\beta]}, \tag{10}$$

with θ the elevation of the scattered wave propagation direction from the horizontal plane, ϕ the scattered wave azimuth (see Fig. 1), ϕ_0 the fast-axis azimuth, and $F_S^{FF}(\theta,\phi,\phi_b,\phi_0)$ the radiation pattern for the scattered transverse component generated by a transverse isotropic inclusion, given by

$$F_S^{FF}(\theta,\phi,\phi_b,\phi_0) = \sin\theta\left[\cos^2\theta\sin 2(\phi-\phi_0) + \sin^2\theta\sin 2(\phi_b-\phi_0)\right]. \tag{11}$$

Using eqns (9) and (10) we can establish the far-field contribution $\delta S_S^{FF}(\mathbf{r}_0;\mathbf{r})$ of a scattering point located at $\mathbf{r}$ to the splitting intensity recorded by a receiver located at $\mathbf{r}_0$ for a monochromatic S wave (Favier & Chevrot 2003):

$$\delta S_S^{FF}(\mathbf{r}_0;\mathbf{r}) = -2Re\left(\frac{\int \delta u_S^{T,FF}(\mathbf{r}_0,t;\mathbf{r})\dot{u}^{R*}(\mathbf{r}_0,t)dt}{\int \dot{u}^R(\mathbf{r}_0,t)\dot{u}^{R*}(\mathbf{r}_0,t)dt}\right) \tag{12}$$

$$= -\gamma\frac{\omega}{2\pi\beta^2 r}F_S^{FF}(\theta,\phi,\phi_b,\phi_0)\sin\left[\frac{\omega(r+z_0-z)}{\beta}\right]. \tag{13}$$

For an *SKS* waveform given by the second derivative of a Gaussian, the spectrum $|u_R(\omega)|^2$ of the incident wave is:

$$|u_R(\omega)|^2 = \frac{\omega^4\tau^2}{4\pi}e^{-\frac{\omega^2\tau^2}{8\pi^2}}, \tag{14}$$

where τ is the characteristic period of the wave. Introducing (14) into (12) leads to (Gradshteyn & Ryzhik 1965, FI II 743 and WH, ET I74(23)):

$$\delta S_S^{FF}(\mathbf{r}_0;\mathbf{r}) = -\gamma\frac{1}{2\pi\beta^2 r}F_S^{FF}(\theta,\phi,\phi_b,\phi_0)\frac{\int\omega^3|u_R(\omega)|^2\sin\left[\frac{\omega(r+z_0-z)}{\beta}\right]d\omega}{\int\omega^2|u_R(\omega)|^2 d\omega} \tag{15}$$

$$= -\gamma \frac{1}{2\pi\beta^2 r} F_S^{FF}(\theta, \phi, \phi_b, \phi_0) \frac{\int \omega^7 \sin\left[\frac{\omega(r+z_0-z)}{\beta}\right] e^{-\frac{\omega^2\tau^2}{8\pi^2}} d\omega}{\int \omega^6 e^{-\frac{\omega^2\tau^2}{8\pi^2}} d\omega} \tag{16}$$

$$= \gamma \frac{1}{4\pi\beta^2 r} F_S^{FF}(\theta, \phi, \phi_b, \phi_0) \frac{1}{30\sqrt{2}} \frac{\pi}{\tau} H_7(a) e^{-a^2} \tag{17}$$

where $H_7(a)$ is the seventh-order Hermite polynomial

$$H_7(a) = 128a^7 - 1344a^5 + 3360a^3 - 1680a$$

and

$$a = \sqrt{2}\frac{(r + z_0 - z)\pi}{\beta\tau}$$

The terms z and z_0 correspond to the third component of $\mathbf{r}$ and $\mathbf{r}_0$ respectively, so that a is directly proportional to the path difference between the S wave scattered at $\mathbf{r}$ and the direct wave. The splitting intensity at receiver point $\mathbf{r}_0$ results from the contribution of each possible scattering point in the medium:

$$S_S^{FF}(\mathbf{r}_0) = \int_V \delta S_S^{FF}(\mathbf{r}_0; \mathbf{r})\, d^3\mathbf{r}.$$

Introducing the two parameters γ_c and γ_s as before leads to:

$$S_S^{FF}(\mathbf{r}_0) = \int_V \left[K_{S,\gamma_c}^{FF}(\mathbf{r}_0; \mathbf{r})\gamma_c(\mathbf{r}) + K_{S,\gamma_s}^{FF}(\mathbf{r}_0; \mathbf{r})\gamma_s(\mathbf{r})\right] d^3\mathbf{r}.$$

Here $K_{S,\gamma_c}^{\mathrm{FF}}$, the sensitivity kernel for parameter γ_c, is given by:

$$K_{S,\gamma_c}^{FF}(\mathbf{r}_0; \mathbf{r}) = \frac{1}{4\pi\beta^2 r} \sin\theta \left(\cos^2\theta \sin 2\phi + \sin^2\theta \sin 2\phi_b\right) \frac{1}{30\sqrt{2}} \frac{\pi}{\tau} H_7(a) e^{-a^2}.$$

Similarly K_{S,γ_s}^{FF}, the sensitivity kernel for parameter γ_s, is given by:

$$K_{S,\gamma_s}^{FF}(\mathbf{r}_0; \mathbf{r}) = -\frac{1}{4\pi\beta^2 r} \sin\theta \left(\cos^2\theta \cos 2\phi + \sin^2\theta \cos 2\phi_b\right) \frac{1}{30\sqrt{2}} \frac{\pi}{\tau} H_7(a) e^{-a^2}.$$

These sensitivity kernels obtained by Favier & Chevrot (2003) are very efficient from the point of view of numerical calculations.

This derivation can be generalized to the other contributions to the Green's tensor. For the other contributions, the sensitivity kernels take the form:

$$K(\mathbf{r}_0; \mathbf{r}) = \mathcal{A} F(\theta, \phi, \phi_b) \frac{1}{r^n} H_{8-n}(x) e^{-x^2}, \tag{18}$$

where $\mathcal{A}$ is a multiplicative factor, F the radiation pattern, n the radial dependence exponent, $8 - n$ the order of the Hermite polynomial defined by (Lebedev 1972, p. 60):

$$H_m(x) = \sum_{k=0}^{m/2} \frac{(-1)^k m!}{k!(m-2k)!} (2x)^{m-2k}.$$

Here x represents the path difference between the scattered and the direct waves, such that x equals a or b for the scattered S wave or P wave, respectively:

$$a = \sqrt{2}\frac{(r + z_0 - z)\pi}{\beta\tau} \tag{19}$$

and

$$b = \sqrt{2}\left(\frac{r}{\alpha} + \frac{z_0 - z}{\beta}\right)\frac{\pi}{\tau}\,. \tag{20}$$

The expressions for the kernels related to each term are presented in Table 1.

Table 1. Splitting intensity sensitivity kernels for γ_c and γ_s, corresponding to the different terms of the Green's tensor. FF represents the far-field kernel, MF the middle-field, NF the near-field and LF the local-field. Subscripts S and P indicate scattered S or P waves, respectively.

Kernel	n	$\mathcal{A}$	$F(\theta, \phi, \phi_b)$	x
K^{FF}_{S,γ_c}	1	$\frac{1}{120\sqrt{2}\beta^2\tau}$	$\sin\theta(\cos^2\theta \sin 2\phi + \sin^2\theta \sin 2\alpha)$	a
K^{FF}_{S,γ_s}	1	$-\frac{1}{120\sqrt{2}\beta^2\tau}$	$\sin\theta(\cos^2\theta \cos 2\phi + \sin^2\theta \cos 2\alpha)$	a
K^{MF}_{S,γ_c}	2	$-\frac{1}{240\pi\beta}$	$\sin\theta[-3\sin 2\phi_b + 6\cos^2\theta(\sin 2\phi_b - \sin 2\phi)]$	a
K^{MF}_{S,γ_s}	2	$-\frac{1}{240\pi\beta}$	$\sin\theta[3\cos 2\phi_b + 6\cos^2\theta(-\cos 2\phi_b + \cos 2\phi)]$	a
K^{NF}_{S,γ_c}	3	$\frac{\tau}{240\sqrt{2}\pi^2}$	$\sin\theta[6\sin 2\phi_b + 15\cos^2\theta(\sin 2\phi - \sin 2\phi_b)]$	a
K^{NF}_{S,γ_s}	3	$-\frac{\tau}{240\sqrt{2}\pi^2}$	$\sin\theta[6\cos 2\phi_b + 15\cos^2\theta(\cos 2\phi - \cos 2\phi_b)]$	a
K^{LF}_{S,γ_c}	4	$\frac{\beta\tau^2}{480\pi^3}$	$\sin\theta[6\sin 2\phi_b + 15\cos^2\theta(\sin 2\phi - \sin 2\phi_b)]$	a
K^{LF}_{S,γ_s}	4	$-\frac{\beta\tau^2}{480\pi^3}$	$\sin\theta[6\cos 2\phi_b + 15\cos^2\theta(\cos 2\phi - \cos 2\phi_b)]$	a
K^{FF}_{P,γ_c}	1	$-\frac{\beta}{120\sqrt{2}\tau\alpha^3}$	$\sin\theta\cos^2\theta(\sin 2\phi_b - \sin 2\phi)$	b
K^{FF}_{P,γ_s}	1	$\frac{\beta}{120\sqrt{2}\tau\alpha^3}$	$\sin\theta\cos^2\theta(\cos 2\phi_b - \cos 2\phi)$	b
K^{MF}_{P,γ_c}	2	$\frac{\beta}{240\alpha^2\pi}$	$\sin\theta[-2\sin 2\phi_b + 6\cos^2\theta(\sin 2\phi_b - \sin 2\phi)]$	b
K^{MF}_{P,γ_s}	2	$\frac{\beta}{240\alpha^2\pi}$	$\sin\theta[2\cos 2\phi_b + 6\cos^2\theta(-\cos 2\phi_b + \cos 2\phi)]$	b
K^{NF}_{P,γ_c}	3	$-\frac{\beta\tau}{240\sqrt{2}\pi^2\alpha}$	$\sin\theta[6\sin 2\phi_b + 15\cos^2\theta(\sin 2\phi - \sin 2\phi_b)]$	b
K^{NF}_{P,γ_s}	3	$\frac{\beta\tau}{240\sqrt{2}\pi^2\alpha}$	$\sin\theta[6\cos 2\phi_b + 15\cos^2\theta(\cos 2\phi - \cos 2\phi_b)]$	b
K^{LF}_{P,γ_c}	4	$-\frac{\beta\tau^2}{480\pi^3}$	$\sin\theta[6\sin 2\phi_b + 15\cos^2\theta(\sin 2\phi - \sin 2\phi_b)]$	b
K^{LF}_{P,γ_s}	4	$\frac{\beta\tau^2}{480\pi^3}$	$\sin\theta[6\cos 2\phi_b + 15\cos^2\theta(\cos 2\phi - \cos 2\phi_b)]$	b

3.2 Complete kernel for splitting intensity

The complete sensitivity kernels K_{γ_c} and K_{γ_s} for splitting intensity are given by the sum of the kernels corresponding to the different contributions to the Green's tensor:

$$
\begin{aligned}
K_{\gamma_c} &= K^{FF}_{P,\gamma_c} + K^{FF}_{S,\gamma_c} + K^{MF}_{P,\gamma_c} + K^{MF}_{S,\gamma_c} + K^{NF}_{S,\gamma_c} + K^{NF}_{P,\gamma_c} + K^{LF}_{S,\gamma_c} + K^{LF}_{P,\gamma_c} \\
&= -\frac{\beta}{120\sqrt{2}\tau\alpha^3}\frac{1}{r}\sin\theta\cos^2\theta(\sin 2\phi_b - \sin 2\phi)e^{-b^2}H_7(b) \\
&\quad + \frac{1}{120\sqrt{2}\tau\beta^2}\frac{1}{r}\sin\theta\left(\cos^2\theta\sin 2\phi + \sin^2\theta\sin 2\phi_b\right)e^{-a^2}H_7(a) \\
&\quad + \frac{\beta}{240\pi\alpha^2}\frac{1}{r^2}\sin\theta\left[-2\sin 2\phi_b + 6\cos^2\theta(\sin 2\phi_b - \sin 2\phi)\right]H_6(b)e^{-b^2} \\
&\quad - \frac{1}{240\pi\beta}\frac{1}{r^2}\sin\theta\left[-3\sin 2\phi_b + 6\cos^2\theta(\sin 2\phi_b - \sin 2\phi)\right]H_6(a)e^{-a^2} \\
&\quad + \frac{\tau}{240\sqrt{2}\pi^2}\frac{1}{r^3}\sin\theta\left[6\sin 2\phi_b + 15\cos^2\theta(\sin 2\phi - \sin 2\phi_b)\right]\left[H_5(a)e^{-a^2} - \frac{\beta}{\alpha}H_5(b)e^{-b^2}\right] \\
&\quad + \frac{\beta\tau^2}{480\pi^3}\frac{1}{r^4}\sin\theta\left[6\sin 2\phi_b + 15\cos^2\theta(\sin 2\phi - \sin 2\phi_b)\right]\left[H_4(a)e^{-a^2} - H_4(b)e^{-b^2}\right] \qquad (21)
\end{aligned}
$$

$$
\begin{aligned}
K_{\gamma_s} &= K^{FF}_{P,\gamma_s} + K^{FF}_{S,\gamma_s} + K^{MF}_{P,\gamma_s} + K^{MF}_{S,\gamma_s} + K^{NF}_{S,\gamma_s} + K^{NF}_{P,\gamma_s} + K^{LF}_{S,\gamma_s} + K^{LF}_{P,\gamma_s} \\
&= \frac{\beta}{120\sqrt{2}\tau\alpha^3}\frac{1}{r}\sin\theta\cos^2\theta(\cos 2\phi_b - \cos 2\phi)e^{-b^2}H_7(b) \\
&\quad - \frac{1}{120\sqrt{2}\beta^2\tau}\frac{1}{r}\sin\theta\left(\cos^2\theta\cos 2\phi + \sin^2\theta\cos 2\phi_b\right)e^{-a^2}H_7(a) \\
&\quad + \frac{\beta}{240\pi\alpha^2}\frac{1}{r^2}\sin\theta\left[2\cos 2\phi_b + 6\cos^2\theta(-\cos 2\phi_b + \cos 2\phi)\right]H_6(b)e^{-b^2} \\
&\quad - \frac{1}{240\pi\beta}\frac{1}{r^2}\sin\theta\left[3\cos 2\phi_b + 6\cos^2\theta(-\cos 2\phi_b + \cos 2\phi)\right]H_6(a)e^{-a^2} \\
&\quad - \frac{\tau}{240\sqrt{2}\pi^2}\frac{1}{r^3}\sin\theta\left[6\cos 2\phi_b + 15\cos^2\theta(\cos 2\phi - \cos 2\phi_b)\right]\left[H_5(a)e^{-a^2} - \frac{\beta}{\alpha}H_5(b)e^{-b^2}\right] \\
&\quad - \frac{\beta\tau^2}{480\pi^3}\frac{1}{r^4}\sin\theta\left[6\cos 2\phi_b + 15\cos^2\theta(\cos 2\phi - \cos 2\phi_b)\right]\left[H_4(a)e^{-a^2} - H_4(b)e^{-b^2}\right] \qquad (22)
\end{aligned}
$$

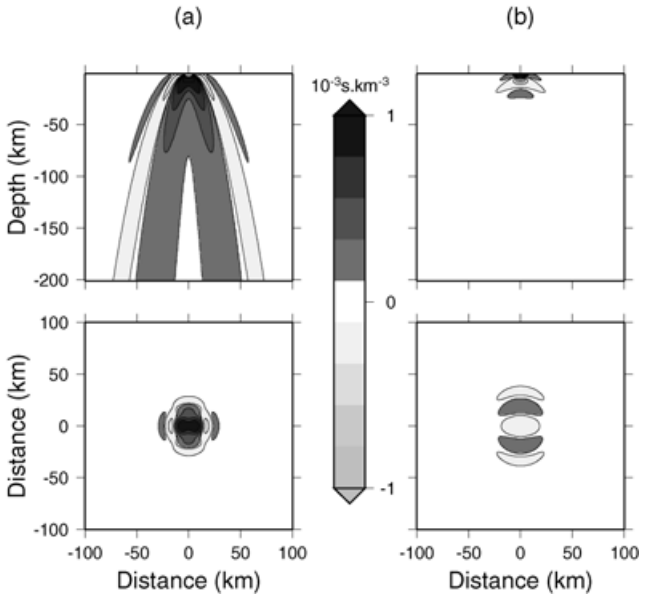

Figure 2. Full sensitivity kernels for splitting intensity for transverse isotropic elastic perturbations vertical cross-sections in the plane $\phi = 0^\circ$ (top) and horizontal cross-sections at a depth of 12 km (bottom). The computation assumes a vertically incident plane *SKS* wave with a characteristic period $\tau = 8$ s, a shear wave velocity $\beta = 4.9$ km s^{-1}, and a receiver located at the surface at the origin. The left and the right plots represent the *S* and *P* contributions to the kernels, respectively. The reference wave polarization is $\phi_b = 0^\circ$ and the fast-axis azimuth is $\phi_0 = -45^\circ$.

so that the splitting intensity measured at the receiver is given by:

$$S(\mathbf{r}_0) = \int_V \gamma_c(\mathbf{r}) K_{\gamma_c}(\mathbf{r}_0; \mathbf{r})\, d^3\mathbf{r} + \int_V \gamma_s(\mathbf{r}) K_{\gamma_s}(\mathbf{r}_0; \mathbf{r})\, d^3\mathbf{r}.$$

The sensitivity kernels for splitting intensity are computed for a shear wave velocity $\beta = 4.9$ km s^{-1} and a characteristic period $\tau = 8$ s, so that the characteristic wavelength is $\lambda = 39$ km. The kernels are plotted in Fig. 2(a) for the *S*-wave contribution and in Fig. 2(b) for the *P*-wave contribution. Far from the receiver, sensitivity kernels remain unchanged from those presented in Favier & Chevrot (2003). However, important differences occur near the receiver where the middle-field and near-field terms are dominant. Over the first 80 km the sensitivity to splitting intensity is no longer zero exactly on the ray path. On the ray, $a = 0$ and the Hermite polynomials are non-zero only for even orders n. However, the local-field and middle-field sensitivity kernels that have Hermite polynomials of odd order n are non-zero along the ray path. The full kernel shown in Fig. 2(a) is more complicated than its far-field approximation. It can no longer be described by concentric rings with alternatively positive crests and negative troughs.

Fig. 3 shows the contributions of each term. The different contributions to the Green's tensor sample the medium at different depth and distance intervals. For each contribution, both the depth and the width of the high sensitivity region decrease from the far-field to the local-field. Moreover, the envelope of the amplitude of the kernels decays exponentially with the square of the difference between the scattered wave and the reference wave traveltimes. If the *S* to *P* scattering occurs far from the receiver, then the difference in traveltimes is large and the kernel vanishes. Consequently, the limiting depth of the sensitivity regions is always larger for scattered *S* waves than for scattered *P* waves, making the *P*-wave sensitivity small everywhere except in the vicinity of the receiver.

3.3 Complete kernels for the *P*- and *S*-wave delay times

3.3.1 Kernel for the S-wave delay time

Here we follow the same approach to derive sensitivity kernels for finite-frequency traveltimes. Keeping density ρ constant, we investigate the effect of velocity perturbations on time delays. Perturbations are introduced in the wave equation as:

$$\lambda \to \lambda + \delta\lambda, \tag{23}$$

$$\mu \to \mu + \delta\mu. \tag{24}$$

These perturbations modify the body wave velocities as follows

$$\frac{\delta\beta}{\beta} = \frac{1}{2}\frac{\delta\mu}{\mu}$$

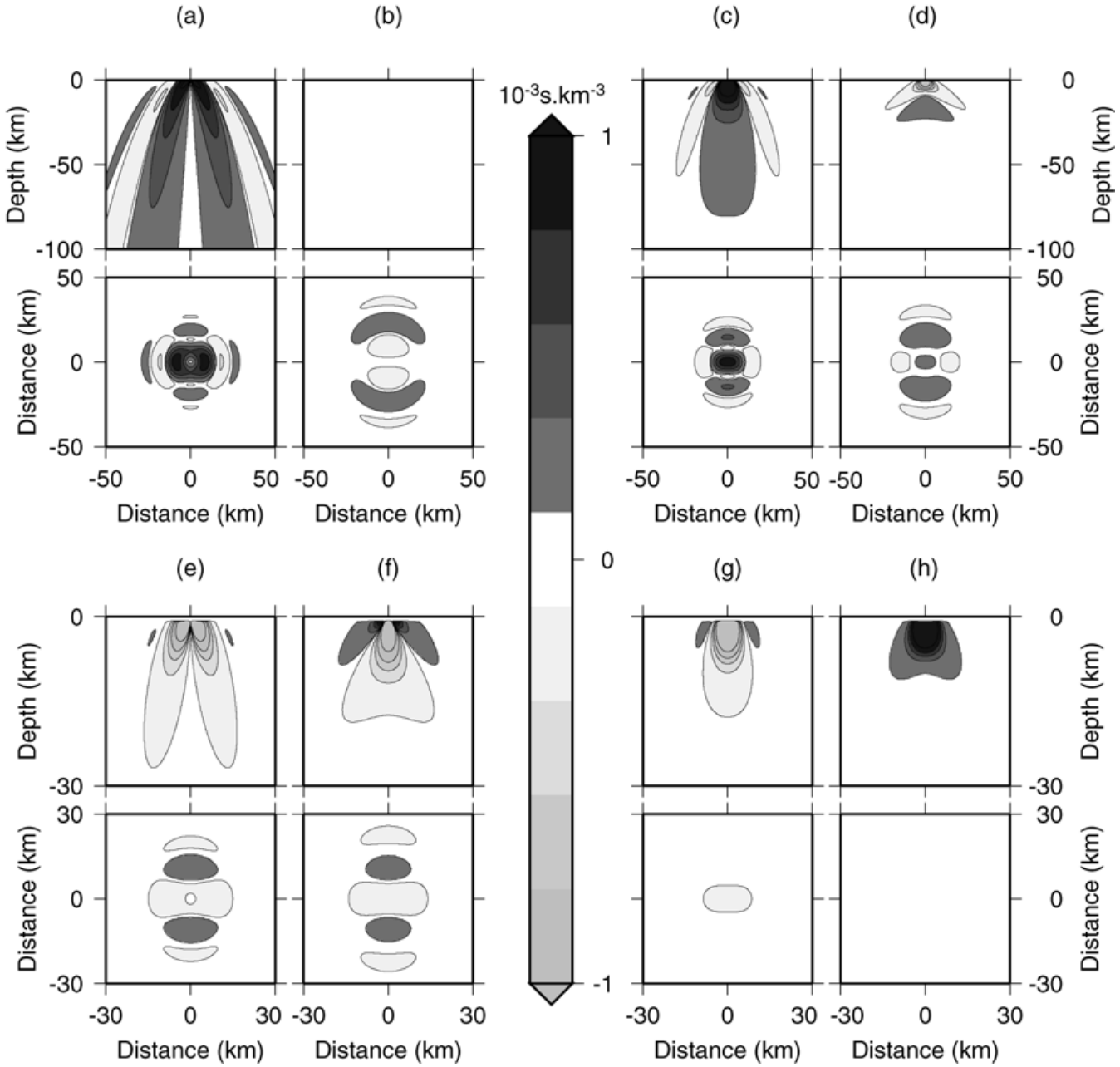

Figure 3. Sensitivity kernels of splitting intensity for each term of the Green's tensor. The experimental configurations are the same as in Fig. 2 with: (a) far-field *S* wave, (b) far-field *P* wave, (c) middle-field *S* wave, (d) middle-field *P* wave, (e) near-field *S* wave, (f) near-field *P* wave, (g) local-field *S* wave, and (h) local-field *P* wave.

and

$$\frac{\delta\alpha}{\alpha} = \frac{1}{2}\frac{\delta\lambda + 2\delta\mu}{\lambda + 2\mu}.$$

We have:

$$\delta T = \frac{\int \delta u^R(t)\dot{u}^R(t)dt}{\int \ddot{u}^R(t)u^R(t)dt} = \mathrm{Re}\left[\frac{\int i\omega\delta u^R(\omega)u_0^{R*}(\omega)d\omega}{\int \omega^2|u_0^R(\omega)|^2 d\omega}\right]. \tag{25}$$

We consider an *S* wave propagating vertically in an isotropic medium. Without loss of generality, the displacement field at point **r** and time *t* can be written in complex notation as:

Table 2. *S*-wave delay time sensitivity kernels for β, corresponding to the different terms of the Green's tensor. FF represents the far-field terms, MF the middle-field, NF the near-field and LF the local-field. Subscripts *SS* and *SP* indicate scattered *S* or *P* waves, respectively, for an incoming *S* wave.

Kernel	n	$\mathcal{B}$	$F(\theta, \phi)$	x
$K^{FF}_{SS,\beta}$	1	$-\frac{1}{120\sqrt{2}\beta^3\tau}$	$\sin\theta(2\cos^2\theta\cos^2\phi - 1)$	a
$K^{FF}_{SP,\beta}$	1	$\frac{1}{120\sqrt{2}\alpha^3\tau}$	$2\sin\theta\cos^2\theta\cos^2\phi$	b
$K^{MF}_{SS,\beta}$	2	$-\frac{1}{240\pi\beta^2}$	$\sin\theta(12\cos^2\theta\cos^2\phi - 3)$	a
$K^{MF}_{SP,\beta}$	2	$\frac{1}{240\pi\alpha^2}$	$\sin\theta(12\cos^2\theta\cos^2\phi - 2)$	b
$K^{NF}_{SS,\beta}$	3	$-\frac{\tau}{240\sqrt{2}\beta\pi^2}$	$\sin\theta(30\cos^2\theta\cos^2\phi - 6)$	a
$K^{NF}_{SP,\beta}$	3	$\frac{\tau}{240\sqrt{2}\alpha\pi^2}$	$\sin\theta(30\cos^2\theta\cos^2\phi - 6)$	b
$K^{LF}_{SS,\beta}$	4	$-\frac{\tau^2}{480\pi^3}$	$\sin\theta(30\cos^2\theta\cos^2\phi - 6)$	a
$K^{LF}_{SP,\beta}$	4	$\frac{\tau^2}{480\pi^3}$	$\sin\theta(30\cos^2\theta\cos^2\phi - 6)$	b

$$\mathbf{u}^R(\mathbf{r}, t) = \begin{pmatrix}1\\0\\0\end{pmatrix} u_0^R(\mathbf{r}, t) = \begin{pmatrix}1\\0\\0\end{pmatrix} u_0 e^{i\omega(t+z/\beta)}.$$

Using the total Green's tensor, we can express the contribution of each tensor component to the scattered perturbed displacement field. In general, the Fréchet kernels take the form:

$$K(\mathbf{r}_0, \mathbf{r}) = \mathcal{B}F(\theta, \phi)\frac{1}{r^n}H_{8-n}(x)e^{-x^2} \tag{26}$$

with $\mathcal{B}$ the multiplicative factor, F the radiation pattern and n the radial dependence exponent. The order of the Hermite polynomial is $8 - n$. Variable x characterizes the path difference between the scattered and the direct waves and should be a, b (eqs 19 and 20), c or d with:

$$c = \sqrt{2}\left(\frac{r + z_0 - z}{\alpha}\right)\frac{\pi}{\tau}$$

and

$$d = \sqrt{2}\left(\frac{r}{\beta} + \frac{z_0 - z}{\alpha}\right)\frac{\pi}{\tau}.$$

Complete expressions of the kernels related to each term are presented in Table 2.

We obtain the global sensitivity kernel of *S*-wave delay time to the perturbation in shear wave velocity:

$$K_{S,\beta} = K^{FF}_{SS,\beta} + K^{FF}_{SP,\beta} + K^{MF}_{SS,\beta} + K^{MF}_{SP,\beta} + K^{NF}_{SS,\beta} + K^{NF}_{SP,\beta} + K^{LF}_{SS,\beta} + K^{LF}_{SP,\beta} \tag{27}$$

$$\begin{aligned}
&= -\frac{1}{120\sqrt{2}\beta^3\tau}\frac{1}{r}\sin\theta\left(2\cos^2\theta\cos^2\phi - 1\right)H_7(a)e^{-a^2}\\
&\quad + \frac{1}{120\sqrt{2}\alpha^3\tau}\frac{1}{r}2\sin\theta\cos^2\theta\cos^2\phi H_7(b)e^{-b^2}\\
&\quad - \frac{1}{240\pi\beta^2}\frac{1}{r^2}\sin\theta\left(12\cos^2\theta\cos^2\phi - 3\right)H_6(a)e^{-a^2}\\
&\quad + \frac{1}{240\pi\alpha^2}\frac{1}{r^2}\sin\theta\left(12\cos^2\theta\cos^2\phi - 2\right)H_6(b)e^{-b^2}\\
&\quad - \frac{\tau}{240\sqrt{2}\pi^2\beta}\frac{1}{r^3}\sin\theta\left(30\cos^2\theta\cos^2\phi - 6\right)\left[H_5(a)e^{-a^2} - \frac{\beta}{\alpha}H_5(b)e^{-b^2}\right]\\
&\quad - \frac{\tau^2}{480\pi^3}\frac{1}{r^4}\sin\theta\left(30\cos^2\theta\cos^2\phi - 6\right)\left[H_4(a)e^{-a^2} - H_4(b)e^{-b^2}\right].
\end{aligned} \tag{28}$$

The total *S*-wave delay time is then given by:

$$\delta T_S = \int_V \delta\beta(\mathbf{r})K_{S,\beta}(\mathbf{r}_0; \mathbf{r})\, d^3\mathbf{r}.$$

Let us note that a first-order change in *P*-wave velocity does not create any *S* to *P* conversion, as shown by Aki & Richards (1980). Consequently, shear wave delay time is not sensitive to a perturbation of *P*-wave velocity. The full kernel is represented in Fig. 4 for an *S* wave with a wavelength $\lambda = 39$ km. The cross-sections of the *S*-wave contribution (Fig. 4a) show that, far from the receiver, the kernel displays concentric rings with alternative signs and vanishes along the ray path. This result has already been established by Dahlen *et al.* (2000) in the far-field approximation. Near the receiver, the kernel is more complicated: sensitivity varies rapidly in space and no longer vanishes on the ray path.

The *P*-wave contribution sensitivity kernel (Fig. 4b) has a very different shape. Concentrated near the receiver, its magnitude decreases rapidly far from the receiver. Nevertheless, this kernel is wider than the previous one at shallow depth. Near the receiver, the sensitivity along

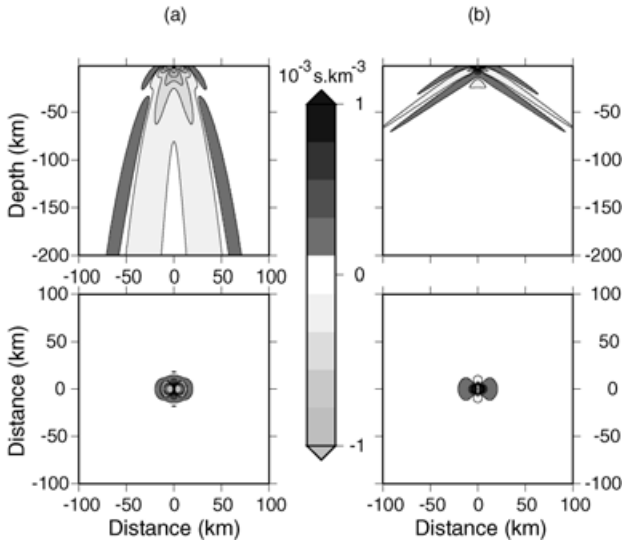

Figure 4. Vertical cross-sections in the plane $\phi = 0^\circ$ (top) and horizontal cross-sections at a depth of 12 km of the exact sensitivity kernels of the *S*-wave delay time for isotropic shear wave velocity perturbations. The computation assumes a vertically incident plane *S* wave with a characteristic period $\tau = 8$ s, a shear wave velocity $\beta = 4.9$ km s^{-1}, and a receiver located at the surface at the origin. Sub-figures (a) and (b) represent *S* and *P* scattered wave contributions, respectively.

the ray path alternates with positive and negative amplitudes. For both kernels, the shape is not invariant to rotation in the horizontal plane and is strongly influenced by the initial polarization of the incident *S* wave.

3.3.2 Kernel for the P-wave delay time

We now consider a vertically incident *P* wave. The wavefield at point **r** and at time *t* is given by:

$$\mathbf{u}^P(\mathbf{r}, t) = \begin{pmatrix} 0 \\ 0 \\ 1 \end{pmatrix} u_0^P(\mathbf{r}, t) = \begin{pmatrix} 0 \\ 0 \\ 1 \end{pmatrix} u_0 e^{i\omega(t+z/\beta)}. \tag{3.3.2}$$

Following the same steps as in the previous section, we can derive the complete Fréchet kernel for *P*-wave delay time as a function of the two model parameters α and β. The results are given in Table 3.

$$K_\alpha = K^{FF}_{PP,\alpha} + K^{MF}_{PP,\alpha}$$
$$= \frac{1}{120\sqrt{2}\alpha^3\tau}\frac{1}{r}\sin\theta H_7(c)e^{-c^2} \tag{29}$$
$$+ \frac{1}{240\pi\alpha^2}\frac{1}{r^2}\sin\theta H_6(c)e^{-c^2} \tag{30}$$

Table 3. *P*-wave delay time sensitivity kernels for α and β corresponding to the different terms of the Green's tensor. FF represents the far-field terms, MF the middle-field, NF the near-field and LF the local-field. Subscripts *PS* and *PP* indicate scattered *S* or *P* waves, respectively, for an incoming *P* wave.

Kernel	n	$\mathcal{B}$	$F(\theta)$	x
$K^{FF}_{PP,\alpha}$	1	$\frac{1}{120\sqrt{2}\alpha^3\tau}$	$\sin\theta$	c
$K^{FF}_{PP,\beta}$	1	$\frac{\beta}{60\sqrt{2}\alpha^4\tau}$	$\sin\theta\cos^2\theta$	c
$K^{FF}_{PS,\beta}$	1	$\frac{1}{60\sqrt{2}\alpha\beta^2\tau}$	$\sin\theta\cos^2\theta$	d
$K^{MF}_{PP,\alpha}$	2	$\frac{1}{240\pi\alpha^2}$	$\sin\theta$	c
$K^{MF}_{PP,\beta}$	2	$-\frac{\beta}{120\pi\alpha^3}$	$\sin\theta(6\cos^2\theta - 2)$	c
$K^{MF}_{PS,\beta}$	2	$\frac{1}{120\pi\alpha\beta}$	$\sin\theta\,(6\cos^2\theta - 2)$	d
$K^{NF}_{PP,\beta}$	3	$-\frac{\tau\beta}{240\sqrt{2}\pi^2\alpha^2}$	$\sin\theta(15\cos^2\theta - 6)$	c
$K^{NF}_{PS,\beta}$	3	$-\frac{\tau}{480\sqrt{2}\pi^2\alpha}$	$\sin\theta(15\cos^2\theta - 6)$	d
$K^{LF}_{PP,\beta}$	4	$-\frac{\tau^2\beta}{240\pi^3\alpha}$	$\sin\theta(15\cos^2\theta - 6)$	c
$K^{LF}_{PS,\beta}$	4	$\frac{\tau^2\beta}{240\pi^3\alpha}$	$\sin\theta(15\cos^2\theta - 6)$	d

and

$$K_\beta = K^{FF}_{PP,\beta} + K^{MF}_{PP,\beta} + K^{NF}_{PP,\beta} + K^{LF}_{PP,\beta} + K^{FF}_{PS,\beta} + K^{MF}_{PS,\beta} + K^{NF}_{PS,\beta} + K^{LF}_{PS,\beta} \tag{31}$$

$$\begin{aligned}
&= \frac{\beta}{60\sqrt{2}\alpha^4\tau}\frac{1}{r}\sin\theta\frac{\beta}{\alpha^2}\cos^2\theta H_7(c)e^{-c^2} \\
&\quad + \frac{1}{60\sqrt{2}\alpha\beta^2\tau}\frac{1}{r}\sin\theta\cos^2\theta H_7(d)e^{-d^2} \\
&\quad - \frac{\beta}{120\pi\alpha^3}\frac{1}{r^2}\sin\theta(6\cos^2\theta - 2)H_6(c)e^{-c^2} \\
&\quad + \frac{1}{120\pi\alpha\beta}\frac{1}{r^2}\sin\theta(6\cos^2\theta - 2)H_6(d)e^{-d^2} \\
&\quad - \frac{\tau}{\pi^2}\frac{1}{\alpha}\frac{1}{480\sqrt{2}}\frac{1}{r^3}\sin\theta\left(15\cos^2\theta - 6\right)H_5(d)e^{-d^2} \\
&\quad - \frac{\tau}{\pi^2}\frac{\beta}{\alpha^2}\frac{1}{240\sqrt{2}}\frac{1}{r^3}\sin\theta\left(15\cos^2\theta - 6\right)H_5(c)e^{-c^2} \\
&\quad - \frac{\tau^2}{240\pi^3}\frac{\beta}{\alpha}\frac{1}{r^4}\sin\theta\left(15\cos^2\theta - 6\right)H_4(c)e^{-c^2} \\
&\quad + \frac{\tau^2}{240\pi^3}\frac{\beta}{\alpha}\frac{1}{r^4}\sin\theta\left(15\cos^2\theta - 6\right)H_4(d)e^{-d^2}.
\end{aligned} \tag{32}$$

The delay time for a P wave propagating in an isotropic medium is then given by:

$$\delta T(\mathbf{r}_0) = \int_V \delta\alpha(\mathbf{r})K_\alpha(\mathbf{r}_0;\mathbf{r})\,d^3\mathbf{r} + \int_V \delta\beta(\mathbf{r})K_\beta(\mathbf{r}_0;\mathbf{r})\,d^3\mathbf{r}.$$

As for the S-wave delay time, a first-order change in P-wave velocity does not create any P to S conversion. Therefore, scattered S waves do not contribute to the delay time measured for a P-wave speed perturbation. The two kernels are represented in Figs 5(a) and (b) for an incident P wave with a characteristic wavelength $\lambda = 68$ km. In Fig. 5(a), we see that perturbations of S-wave velocities only influence P-wave delay time near the receiver and do not have any effect far from the receiver. Near the receiver, this kernel exhibits concentric rings with alternatively positive and negative amplitudes. Moreover, it is no longer zero along the ray path. In Fig. 5(b), the sensitivity kernel to P-wave velocity perturbations consists in concentric rings with opposite signs. As for S waves, sensitivity is no longer zero along the ray path due to the near-field terms at shallow depth. The P kernels exhibit a cylindrical symmetry in the horizontal plane, as expected for P-wave propagation in an isotropic medium. This result is confirmed by the analytical expressions of the sensitivity kernels, which do not depend on azimuth.

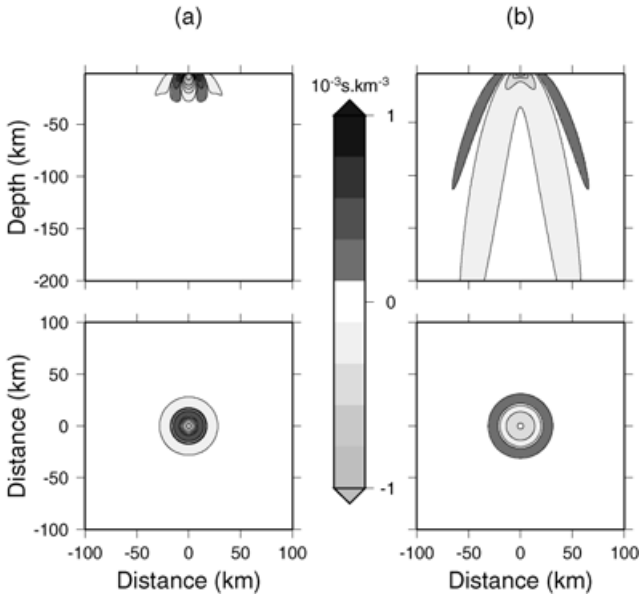

Figure 5. Vertical cross-sections in the plane $\phi = 0^\circ$ (top) and horizontal cross-sections at a depth of 12 km of the exact sensitivity kernels for P-wave delay time for (a) S-wave velocity perturbations and (b) P-wave velocity perturbations. The computation assumes a vertically incident P wave with a characteristic period $\tau = 8$ s, a P-wave velocity $\alpha = 8.5$ km s^{-1}, a shear velocity $\beta = 4.9$ km s^{-1}, and a receiver located at the surface at the origin.

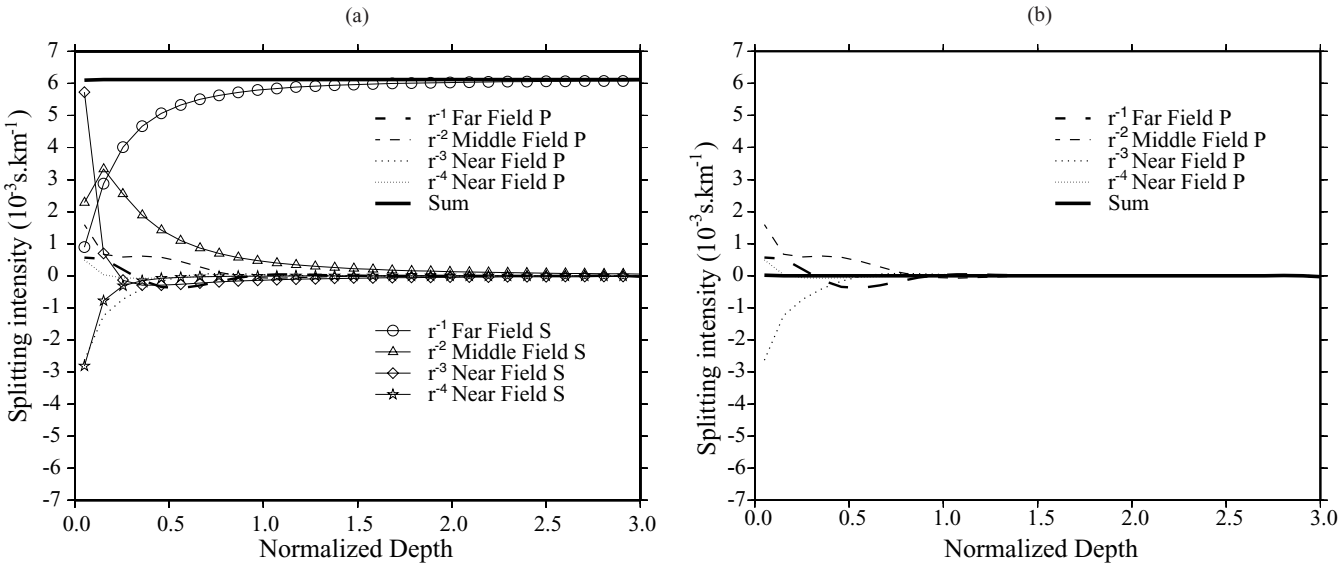

Figure 6. Contribution of the different terms of the Green's tensor to splitting intensity per unit length (in s km^{-1}) for a homogeneous hexagonal anisotropic layer with azimuth $\phi_0 = -45°$. We consider the case of a plane S wave with $\phi_b = 0°$, a shear wave velocity $\beta = 4.9$ km s^{-1}, a characteristic period $\tau = 8$ s and 3 per cent anisotropy. Sub-figure (a) represents all the contributions and (b) represents only P scattered waves contributions. The theoretical value given by ray theory is 6.1 ms. The thick solid line represents the sum of all the contributions.

4 SENSITIVITY AS A FUNCTION OF DEPTH

To check the validity of the analytical expressions of sensitivity kernels, we compute the sum of the kernels in a laterally homogeneous horizontal plane at depth z. The integrals for both splitting intensity and delay time as a function of depth give:

$$\delta S(z) = \gamma_c(z) \int_S K_{\gamma_c}(\mathbf{r}_0, \mathbf{r})\, dS + \gamma_s(z) \int_S K_{\gamma_s}(\mathbf{r}_0, \mathbf{r})\, dS \qquad 4$$

and

$$\delta T(z) = \delta\alpha(z) \int_S K_{\alpha}(\mathbf{r}_0, \mathbf{r})\, dS + \delta\beta(z) \int_S K_{\beta}(\mathbf{r}_0, \mathbf{r})\, dS.$$

Appendix A shows that the result of the integral depends only on the normalized depth z/λ for each term of the sensitivity kernels. The wavelength λ is therefore the appropriate parameter to normalize the depth dependence of the sensitivity kernels.

4.1 Splitting intensity as a function of depth

Fig. 6 compares predictions from kernel integration and classical ray theory. When all the terms of the Green's tensor are taken into account, the kernel gives the exact value predicted by ray theory at all depths. This result can be demonstrated analytically, as shown in Appendix A. Fig. 6(b) represents the P-wave contributions to the Green's tensor. Because the different P contributions cancel, scattered P waves do not contribute to shear wave splitting in a laterally homogeneous, transverse isotropic medium.

It is possible to define zones of influence for near-field, middle-field, and far-field terms for scattered S waves. From the surface to the depth $\lambda/10$, the near-field and local-field terms dominate. From $\lambda/10$ to $\lambda/6$ the middle-field term is the strongest. Beyond $\lambda/6$ the far-field term dominates. Note that the middle-field term, though weak, plays an important role down to a depth of 2λ. As a conclusion, the far-field term can be considered as a good approximation of the Green's tensor only for depths larger than 2λ. For a depth λ, the error introduced by the far-field approximation is less than 5 per cent. This result confirms the hypothesis made in Favier & Chevrot (2003) that the loss of precision in splitting intensity at shallow depth using a far-field approximation results from the use of a far-field Green's tensor.

Thus, we come to the important conclusion that the splitting intensity contribution is constant with depth and agrees with the value expected by classical ray theory $\delta t \sin 2(\phi_b - \phi_0)$ provided the full Green's tensor is taken into account.

4.2 Delay time as a function of depth

4.2.1 Incident S wave

Next, we compute the contribution of a unitary height of the medium to the delay time calculated at the surface in the case of an incident S wave (Fig. 7a). The result agrees with the value expected by ray theory ($\delta T = -\delta\beta/\beta^2$) and is constant with depth (see Appendix A). Note also that the different scattered P-wave contributions cancel (Fig. 7b) and do not contribute to the delay time. Moreover, Fig. 7(b) allows us to define zones of predominance for the different contributions to the Green's tensor. From the surface to the depth $\lambda/10$, the near-field term is

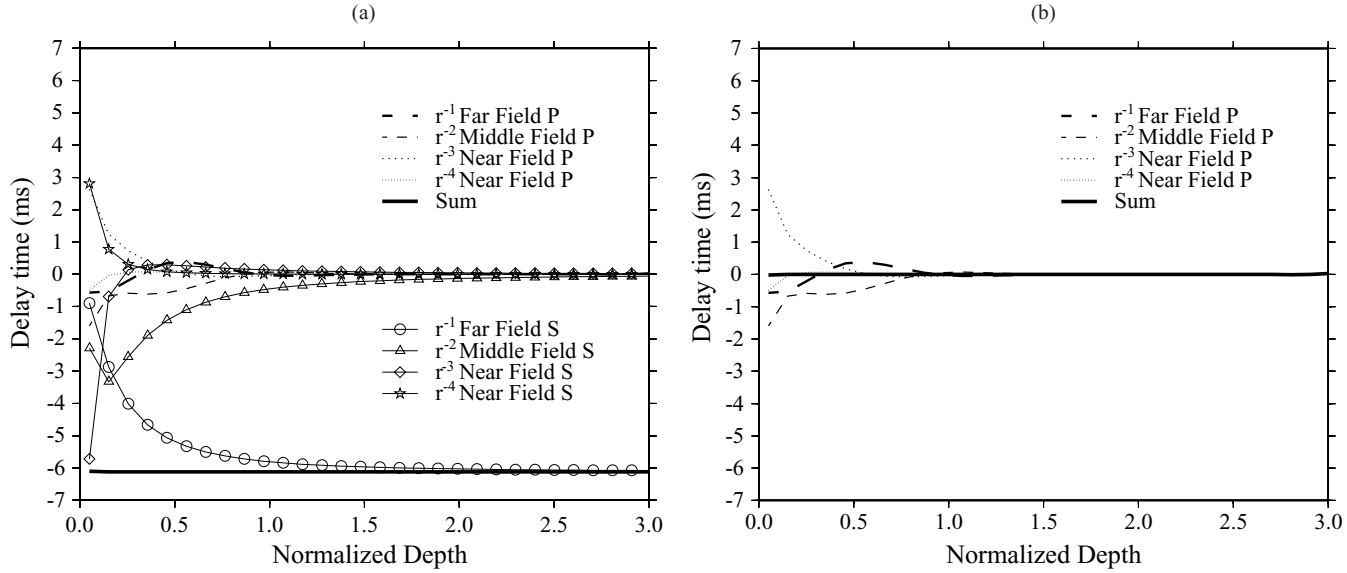

Figure 7. Contribution of the different terms of the Green's tensor to *S*-wave delay time per unit length (in s km^{-1}) for a homogeneous isotropic layer. We consider the same experimental configuration as in Fig. 4. Subfigure (a) represents all contributions to delay time (b) gives only scattered *P*-wave contributions to delay time . The theoretical value given by ray theory is $\delta T = -6.1$ ms. The thick solid line represents the sum of all the contributions.

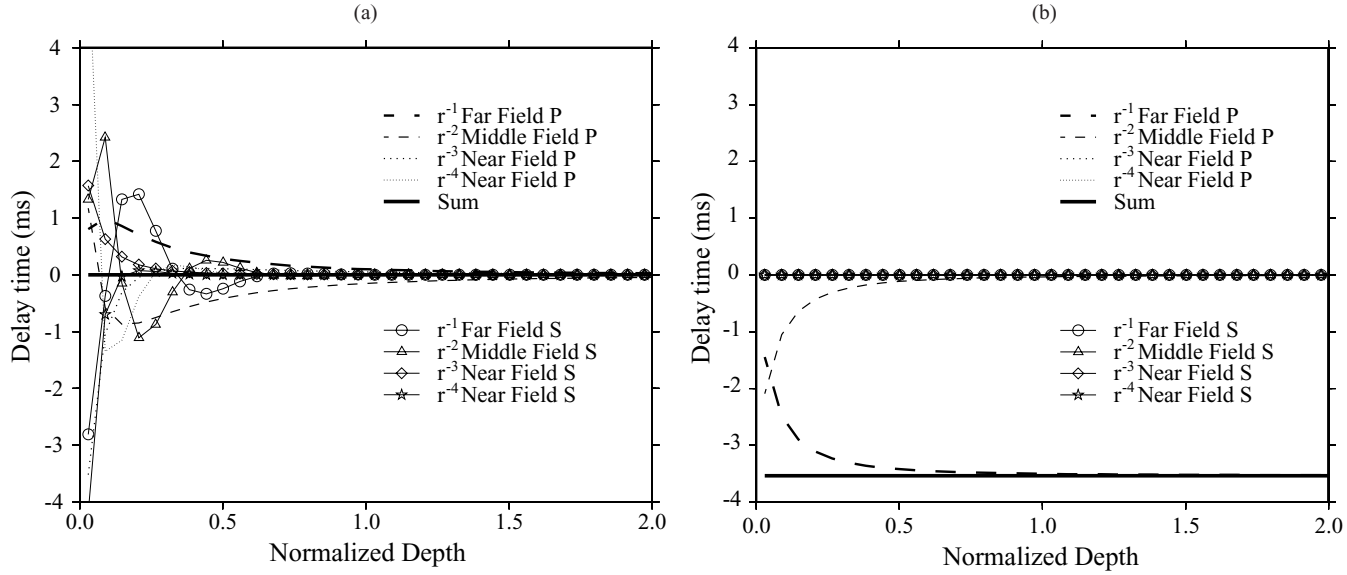

Figure 8. Contribution of the different terms of the Green's tensor to *P*-wave delay time per unit length (in s km^{-1}) for a homogeneous isotropic layer. We consider the same experimental configuration as in Fig. 5. Sub-figure (a) represents all contributions to delay time for a perturbation of 3 per cent of shear wave velocity, (b) represents all contributions to delay time for a perturbation of 3 per cent of *P*-wave velocity. The theoretical value given by ray theory is $\delta T = -3.5$ ms.

the most important. From $\lambda/10$ to $\lambda/6$, the middle-field term dominates. Finally the far-field term becomes predominant for depths larger than $\lambda/6$. However, the middle-field term cannot be neglected up to a depth of 2λ. These zones of influence are the same as for splitting intensity.

4.2.2 Incident P wave

Following the same approach, in Fig. 8 we present results for delay time as a function of depth in the case of an incident *P* wave. The results agree perfectly with ray theory: perturbations of *S*-wave velocity have no influence on *P*-wave traveltime and perturbations of *P*-wave velocity give a constant delay time with depth ($\delta T = -\delta\alpha/\alpha^2$). As expected from (30) and (32), the near-field contribution does not depend on *P*-wave velocity perturbations. Near-field terms only appear in the sensitivity kernel for shear wave velocity perturbations. Moreover, this kernel sums to zero for a homogenous layer. Finally, we can define zones of influence from the surface to $\lambda/20$ for the middle-field terms, and from $\lambda/20$ to infinity for the far-field terms. Nevertheless, considering far-field terms only is not accurate for depths smaller than λ. Therefore, complete sensitivity kernels are required for an accurate calculation between the surface and depth λ.

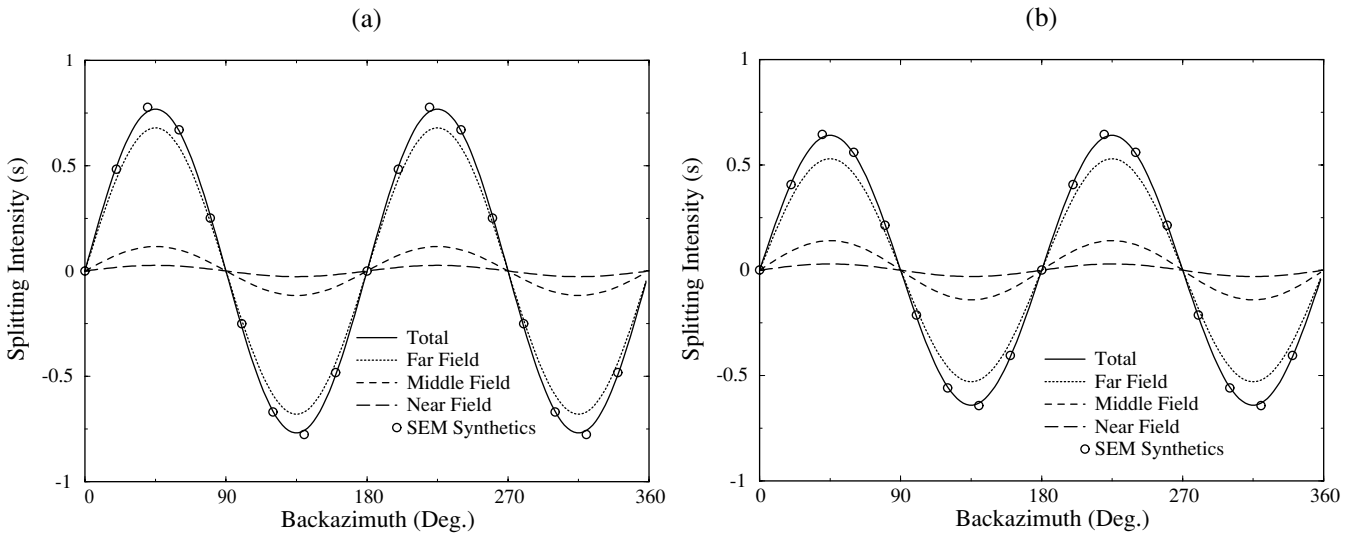

Figure 9. Contribution of the different terms of the Green's tensor to the splitting intensity measured at the surface for a homogeneous anisotropic layer. All contributions to splitting intensity are represented for (a) a perturbation of 3 per cent of shear wave velocity and a layer located between 32 km and 160 km depth, and (b) a perturbation of 5 per cent of shear wave velocity and a layer located between 32 km and 96 km depth. Both anisotropic layers have a fast-axis direction $\phi_0 = 0^\circ$. In both cases we consider an incident plane wave with a characteristic period $\tau = 14$ s and a shear wave velocity $\beta = 5$ km s^{-1}.

5 NUMERICAL MODELLING

We use the spectral-element method (SEM) to compute accurately synthetic seismograms in anisotropic media based on direct numerical resolution of the full wave equation. The method uses a mesh of hexahedral finite elements on which the wavefield is represented in terms of high-degree Lagrange polynomials. The main advantage of the SEM is that it combines the flexibility of the finite-element method with the accuracy of pseudospectral techniques. It is widely used and has been thoroughly validated in the context of seismic wave propagation (e.g. Komatitsch & Vilotte 1998; Komatitsch & Tromp 2002). It can handle a full anisotropic tensor with up to 21 coefficients (Komatitsch *et al.* 2000). Splitting intensity is computed, based on complete sensitivity kernels on the one hand and the analysis of the synthetics computed by the SEM (Chevrot 2000) on the other, for a homogeneous anisotropic layer located at depths between: (i) 32 km and 160 km with 3 per cent anisotropy; and, (ii) 32 km and 96 km with 5 per cent anisotropy. Both have a fast-axis azimuth $\phi_0 = 0^\circ$, the incident plane wave has a characteristic period $\tau = 14$ s and a shear wave velocity $\beta = 5$ km s^{-1}. The comparison, shown in Fig. 9, shows that sensitivity kernels and SEM synthetics are in excellent agreement. This demonstrates that complete sensitivity kernels accurately describe wave propagation in weakly anisotropic media and that higher order terms that would result from multiple scattering can be safely neglected. The small differences observed between the two approaches result from the free surface that is not taken into account in the calculation of the sensitivity kernels. Accordingly we can assume that these effects are even smaller for seismic waves propagating through the Earth's crust because the wave velocity, and consequently the incidence angle, are smaller. On the contrary, middle-field and near-field terms are important since they can introduce errors of the order of 12 per cent for case (i) to 20 per cent for case (ii). The importance of the middle-field and near-field terms increases significantly as the anisotropic layer is located closer to the surface. With the far-field approximation, the fast-axis direction is correctly retrieved but the delay time value is underestimated.

6 CONCLUSION

Using the complete Green's tensor in a reference isotropic medium, we have derived simple analytical expressions for sensitivity kernels for both splitting intensity and delay times for *P* and *S* waves. These kernels provide some physical insights into the limitation of the far-field approximation and the assumptions that are commonly made in seismic tomography.

First, sensitivity for shear wave splitting and delay time is no longer zero along the ray path near the receiver. This is due to middle-field and local-field terms in the Green's tensor expression. Far from the receiver, sensitivity kernels have a shape consisting in concentric rings with alternatively positive and negative sign and a radius that increases with depth and with wavelength. Near the receiver, and by symmetry near the source, the kernel is more complicated as sensitivity varies rapidly over a distance comparable to the wavelength.

Moreover, the zones of influence for the different terms can be defined. They depend only on the wavelength. For *S* waves, the near-field terms dominate up to a depth of $\lambda/10$, then the middle-field term dominates up to $\lambda/6$, beyond which the far-field term becomes dominant. For *P* waves, the middle-field term is dominant up to $\lambda/20$, beyond which the far-field term dominates. However the middle-field term cannot be neglected for depths smaller than 2λ for *S* waves and λ for *P* waves. For example, for an incident *S* wave with a characteristic period $\tau = 20$ s, the far-field approximation is not valid from the surface down to a depth of 200 km. This conclusion holds both near the source and near the

receiver. Sensitivity kernels calculated based on the far-field approximation are not valid from the surface to a limit depth of λ for *P* waves and 2λ for *S* waves. As a result, exact kernels must be used in tomographic studies of the lithosphere that rely on long period body waves.

Sensitivity kernels calculated with normal-mode theory (Zhao *et al.* 2000) take into account near field effects. Although these kernels should give accurate results, their computation is much more expensive and they are typically limited to periods larger than 15 s.

Analytical integration of the kernels gives the exact values predicted by ray theory for both splitting intensity and delay times. Moreover, sensitivity is constant as a function of depth for a laterally homogeneous background medium. We note that scattered *P* waves neither contribute to the *S*-wave delay time nor to splitting intensity, and that scattered *S* waves do not contribute to the *P*-wave delay time in a laterally homogeneous background medium.

ACKNOWLEDGMENTS

The authors are grateful to Dr. Li Zhao and an anonymous reviewer for their careful review and constructive comments that improved the manuscript. We also thank Dr Kurt Feigl for his comments. This research was supported by an INSU grant 'Intérieur de la Terre'. One of the authors DK was supported in part by the United States National Science Foundation.

REFERENCES

Aki, K. & Richards, P.G., 1980. *Quantitative Seismology-Theory and Methods,* Freeman, New York.

Chevrot, S., 2000. Multichannel analysis of shear wave splitting, *J. geophys. Res.,* **105,** 21 579–21 590.

Dahlen, F.A., Hung, S.H. & Nolet, G., 2000. Fréchet kernels for finite-frequency traveltimes-I. Theory,, *Geophys. J. Int.,* **141,** 157–174.

Favier, N. & Chevrot, S., 2003. Sensitivity kernels for shear wave splitting in transverse isotropic media, *Geophys. J. Int.,* **153,** 213–228.

Gradshteyn, I. & Ryzhik, I., 1965. *Table of Integrals, Series, and Products,* Academic Press, New York.

Hung, S.-H., Dahlen, F.A. & Nolet, G., 2000. Fréchet kernels for finite-frequency traveltimes-II. Examples, *Geophys. J. Int.,* **141,** 175–203.

Komatitsch, D. & Tromp, J., 2002. Spectral-element simulations of global seismic wave propagation-I. Validation, *Geophys. J. Int.,* **149,** 390–412.

Komatitsch, D. & Vilotte, J.P., 1998. The spectral-element method: an efficient tool to simulate the seismic response of 2D and 3D geological structures, *Bull. seism. Soc. Am.,* **88**(2), 368–392.

Komatitsch, D., Barnes, C. & Tromp, J., 2000. Simulation of anisotropic wave propagation based upon a spectral element method, *Geophysics,* **65**(4), 1251–1260.

Lebedev, N.N., 1972. *Special Functions and their Applications,* Dover Publication, New York.

Marquering, H., Nolet, G. & Dahlen, F.A., 1998. Three-dimensional waveform sensitivity kernels, *Geophys. J. Int.,* **132,** 521–534.

Marquering, H., Dahlen, F.A. & Nolet, G., 1999. Three-dimensional sensitivity kernels for finite-frequency traveltimes: the banana-doughnut paradox, *Geophys. J. Int.,* **137,** 805–815.

Mensch, T. & Rasolofosaon, P., 1997. Elastic-wave velocities in anisotropic media of arbitrary symmetry—generalization of Thomsen's parameters ϵ, δ and γ, *Geophys. J. Int.,* **128,** 43–64.

Tarantola, A., 1987. Inversion of travel times and seismic waveforms, in *Seismic Tomography,* pp. 135–157, ed. Nolet, G., D. Reidel, Dordrecht.

Zhao, L. & Jordan, T.H., 1998. Sensitivity of frequency-dependent traveltimes to laterally heterogeneous, anisotropic Earth structure, *Geophys. J. Int.,* **133,** 683–704.

Zhao, L., Jordan, T.H. & Chapman, C.H., 2000. Three-dimensional Fréchet differential kernels for seismic delay times, *Geophys. J. Int.,* **141,** 558–576.

APPENDIX A: ANALYTICAL INTEGRATION OF SENSITIVITY KERNELS

In this section we investigate the properties of the integral of the sensitivity kernels at a given depth. We first express the integral of a single term of the kernel over the horizontal plane defined by its depth z, and subsequently generalize it to the other terms. As an example, we integrate the middle-field term of K_α given in (30):

$$I = \int_S K^{MF}_{PP,\alpha}(\mathbf{r})\, dS = \int_S \frac{1}{240\pi\alpha^2}\frac{1}{r^2}\sin\theta H_6(c) e^{-c^2}\, dS, \tag{A1}$$

with

$$c = c\left(\frac{z}{\lambda},\theta\right) = \sqrt{2}\pi\frac{r-z}{\lambda} = \sqrt{2}\pi\frac{1-\sin\theta}{\sin\theta}\frac{z}{\lambda}$$

and

$$dS = -z^2\frac{\cos\theta}{\sin^3\theta}\, d\theta\, d\phi.$$

Therefore:

$$I = \int_0^{2\pi} d\phi \int_0^{\pi/2} \frac{1}{240\pi\alpha^2}\cos\theta H_6\left[c\left(\frac{z}{\lambda},\theta\right)\right] e^{-c^2\left(\frac{z}{\lambda},\theta\right)}\, d\theta$$

and the integral only depends on normalized depth z/λ. Each contribution to the Green's tensor has a similar depth dependence, so that the total sensitivity kernel integrated over the horizontal plane only depends on normalized depth.

The sum of the different contributions to the Green's tensor can be determined analytically. We will detail the case of the sum of K_α for which the expression is given in (30). Let us consider the integral J defined by:

$$J = \int_S K_\alpha(\mathbf{r})\, dS = J_1 + J_2$$

with

$$J_1 = \int_S \frac{1}{120\sqrt{2}\alpha^3\tau}\frac{1}{r}\sin\theta H_7(c)e^{-c^2}dS$$

and

$$J_2 = \int_S \frac{1}{240\pi\alpha^2}\frac{1}{r^2}\sin\theta H_6(c)e^{-c^2}dS.$$

The elementary surface dS is given as a function of c by:

$$dS = \frac{\lambda}{\sqrt{2}\pi}\left[z + \left(\frac{\lambda}{\sqrt{2}\pi}\right)c\right]dc\,d\phi.$$

ϕ varies from 0 to 2π, while c varies from 0 to $+\infty$. We obtain:

$$J_1 = \frac{1}{120\alpha^2}z\int_0^{+\infty}\frac{1}{z+\frac{\lambda}{\sqrt{2}\pi}c}H_7(c)e^{-c^2}dc. \tag{A2}$$

Using the following property of Hermite polynomials (Lebedev 1972, p. 75):

$$e^{-x^2}H_n(x) = -\frac{d}{dx}\left[e^{-x^2}H_{n-1}(x)\right]$$

and integrating (A2) by parts leads to:

$$J_1 = \frac{1}{120\alpha^2}z\left(\left[\frac{-1}{z+\frac{\lambda}{\sqrt{2}\pi}c}H_6(c)e^{-c^2}\right]_0^{+\infty} - \frac{\lambda}{\sqrt{2}\pi}\int_0^{+\infty}\frac{1}{\left(z+\frac{\lambda}{\sqrt{2}\pi}c\right)^2}H_6(c)e^{-c^2}\right).$$

Finally we get:

$$J_1 = \frac{1}{120\alpha^2}H_6(0) - J_2$$

so that:

$$J = \int_S K_\alpha(\mathbf{r})\,dS = -\frac{1}{\alpha^2}.$$

The result does not depend on depth and exactly gives the value predicted by ray theory. The same approach can be used for each sensitivity kernel since it is independent of the order of the Gaussian derivative chosen to represent the source function spectrum. From eqs (28) and (32), we establish that:

$$\int_S K_\beta(\mathbf{r})\,dS = 0$$

$$\int_S K_{S,\beta}(\mathbf{r})\,dS = -\frac{1}{\beta^2}$$

for an incident S wave. Similarly, using eqs (21) and (22), we have for splitting intensity:

$$\int_S K_{\gamma_c}(\mathbf{r})\,dS = \frac{1}{\beta}\sin 2\phi_b$$

$$\int_S K_{\gamma_s}(\mathbf{r})\,dS = -\frac{1}{\beta}\cos 2\phi_b.$$